Research Square

Preprints are preliminary reports that have not undergone peer review.
They should not be considered conclusive, used to inform clinical practice,
or referenced by the media as validated information.

NG2-expressing cells support capillary-rich skeletal muscle homeostasis, and their repeated depletion is associated with increased mortality

Hideaki Sato
Asahikawa Medical University
Takamitsu Tatsukawa
Asahikawa Medical University
Kei-ichi Nakajima
Asahikawa Medical University
Yugo Watanabe
Asahikawa Medical University
Hirofumi Sakuma
Asahikawa Medical University
Yuya Kobayashi
Asahikawa Medical University
Yukari Sakurai
Asahikawa Medical University
Shota Tokuno
Asahikawa Medical University
Yoshinori Minami
Asahikawa Medical University
Yusuke Inoue
Asahikawa Medical University
Takashi Yazawa
Asahikawa Medical University
Masanori Takekawa
Asahikawa Medical University
Jun-ichi Kawabe
kawabeju@asahikawa-med.ac.jp
Asahikawa Medical University

Research Article

Keywords: skeletal muscle, capillary, pericyte, mesenchymal stem cells, sarcopenia, dysphagia, microvascular niche, neuromuscular junction, terminal Schwann cells

Posted Date: October 21st, 2026

DOI: https://doi.org/10.21203/rs.3.rs-10338126/v1

License: This work is licensed under a Creative Commons Attribution 4.0 International License.
Read Full License

Additional Declarations: No competing interests reported.

NG2-expressing cells support capillary-rich skeletal muscle homeostasis, and their repeated depletion is associated with increased mortality

Authors:

Hideaki Sato[1,2],Takamitsu Tatsukawa[1,3], Kei-ichi Nakajima[1], Yugo Watanabe[1], Hirofumi Sakuma[1,4], Yuya Kobayashi[1,4], Yukari Sakurai[1,5], Shota Tokuno[1,4], Yoshinori Minami[6], Yusuke Inoue[7], Takashi Yazawa[1], Masanori Takekawa[2], and Jun-ichi Kawabe[1]

Affiliations:

1. Department of Biochemistry
2. Department of Oral and Maxillofacial Surgery
3. Department of Vascular Surgery
4. Department of Internal Medicine, Division of Cardiology and Nephrology
5. Department of Pediatrics
6. Department of Internal Medicine, Division of Respiratory Medicine and Neurology
7. Advanced Medical Engineering Research Center

Asahikawa Medical University, 2-1-1 Midorigaoka-Higashi, Asahikawa, 078-8510, Japan

Correspondence: Jun-ichi Kawabe

Department of Biochemistry, Asahikawa Medical University, 2-1-1 Midorigaoka-Higashi, Asahikawa 078-8510, Japan.

Tel: +81-166-68-2352, Mail address; kawabeju@asahikawa-med.ac.jp

Keywords: skeletal muscle, capillary, pericyte, mesenchymal stem cells, sarcopenia, dysphagia, microvascular niche, neuromuscular junction, terminal Schwann cells,

Abstract

Background: Skeletal muscle undergoes continuous myonuclear turnover even under steady-state conditions, requiring a sustained supply of new myonuclei to preserve tissue homeostasis. Satellite cells (SCs) play role in skeletal muscle maintenance, but we previously reported that perivascular $NG2^+$ cells also contribute to this process. Replenishment of $NG2^+$ cells after their depletion may mask the consequences of their loss, leaving their roles across muscle groups throughout the body unclear.

Methods: $NG2^+$ cells were conditionally ablated in NG2-CreERT;Rosa26-DTA mice by tamoxifen administration. To minimize compensatory cellular replenishment, $NG2^+$ cell depletion was repeatedly induced bi-monthly. $NG2^+$ cell lineage tracing was performed using NG2-CreERT;Rosa26-tdTomato mice to identify muscle fibers incorporating $NG2^+$ cell-derived myonuclei. Muscle atrophy and regeneration were assessed by histological and transcriptomic analyses. Capillary and $NG2^+$ cell densities were quantified by three-dimensional imaging of optically cleared skeletal muscles from NG2-DsRed mice.

Results: Repeated $NG2^+$ cell-depletion resulted in body weight loss, kyphosis, respiratory abnormalities, and increased mortality. Pulmonary inflammation and airway debris were consistent with pathology related to aspiration pneumonia. Muscle atrophy occurred in slow-twitch limb muscles as well as in the erector spinae and digastric muscles, which are functionally associated with posture and swallowing, respectively. Lineage tracing revealed enrichment of $NG2^+$ cell-derived myofibers in slow-twitch regions of somite-derived muscles and in fast-twitch regions of pharyngeal muscles, including the digastric muscle. $NG2^+$ cell dependency correlated with high capillary density and abundant microvessel-associated $NG2^+$ cells rather than fiber-type identity *per se.* Depleted muscles also exhibited fragmented neuromuscular junctions. Transcriptomics demonstrated downregulation of sarcomeric structure- and neuromuscular junction-related genes, without enhancing canonical hypoxia response pathway.

Conclusions: These findings identify $NG2^+$ cells as indispensable regulators of muscle mass and function in a muscle-specific manner governed by the local microvascular niche. Repeated $NG2^+$ cell-depletion is associated with neuromuscular abnormalities and severe systemic deterioration, highlighting the importance of $NG2^+$ cells in muscles involved in posture and swallowing. Together, these findings establish $NG2^+$ cells as key regulators of skeletal muscle homeostasis and provide a mechanistic framework for understanding the pathogenesis of sarcopenia and developing therapeutic strategies.

Background

Skeletal muscle constitutes around 40% of body weight and accounts for 20% of basal metabolic rate [1]. Beyond its canonical functions in locomotion and postural control, skeletal muscle plays essential roles in metabolism, *e.g.* insulin-dependent glucose disposal, serves as a major reservoir for protein-derived energy, and contributes to thermogenesis. Moreover, myokines secreted by skeletal muscle exert systemic effects, modulating the function of multiple organs as well as immune, metabolic, and neural processes [2]. Skeletal muscle possesses a high regenerative capacity; nevertheless, age-associated declines in muscle mass and strength, termed sarcopenia, have emerged as a major clinical concern [3]. This pathological condition, characterized by impaired intrinsic muscular function, has been associated with reductions in individual independence and quality of life, as well as all-cause mortality [3, 4]. Thus, in aging societies, elucidating strategies to preserve both the quantity and quality of skeletal muscle has become critically important for extending healthy lifespan.

Although multinucleated myofibers appear structurally stable, myonuclear turnover occurs even at steady state, and the balance between myonuclear supply and loss is critical for maintaining myofiber size [5, 6]. It is well recognized that $Pax7^+$ satellite cells (SCs) serve as a principal myogenic stem cell population, and play an essential role in the regeneration and maintenance of skeletal muscle [7-10]. Reductions in the number and functional capacity of SCs have been regarded as primary contributors to the development of sarcopenia [11]. However, conditional cellular depletion studies indicate that SCs are not universally required to maintain adult muscle mass and sarcopenia does not occur under normal steady-state conditions [12]. Notably, certain muscle groups including pharyngeal muscles have been reported to exhibit atrophy when SCs are depleted, suggesting regional heterogeneity in the requirement for SCs in maintaining muscle homeostasis [13, 14]. In any case, SC depletion does not cause overt sarcopenic phenotype, allowing survival throughout their lifespan. These observations suggest that the maintenance and function of skeletal muscles cannot be attributed solely to SCs; rather, their local microenvironmental niche, which involves various cellular populations such as fibro-adipogenic progenitors (FAPs), vascular endothelial cells, and pericytes (PCs) [15-17].

PCs are mural cells embedded within the capillary basement membrane and regulate microvascular integrity and permeability [18]. Beyond their vascular roles, subsets of PCs show mesenchymal stem cel-like multipotency and act function as myogenic progenitor cells [19-22]. In our previous study using NG2-CreERT-based lineage-tracing and depletion models, NG2-lineage cells contributed to skeletal myofibers under homeostatic conditions, particularly in slow-twitch muscles such as the soleus, and depletion of NG2-expressing cells ($NG2^+$ cells) resulted in

selective atrophy of these muscles [23]. Although the perivascular localization of many labeled cells was consistent with the involvement of microvascular PCs, NG2-based genetic systems are not exclusively specific to PC and may also target other $NG2^+$ cell populations. These findings prompted us to investigate the broader role of $NG2^+$ cells, including but not limited to PCs, in the maintenance of skeletal muscles throughout the body and in systemic homeostasis. Because compensatory replenishment of perivascular $NG2^+$ cells has been reported *in vivo* [24, 25], we further reasoned that repeated depletion would be necessary to reveal the consequences of sustained loss of the targeted $NG2^+$ cell population.

In this study, we found that repeated induction of $NG2^+$ cell depletion ultimately resulted in lethality and was associated with fiber-type independent muscular atrophy, thereby elucidating the role of $NG2^+$ cells in muscle groups essential for vital physiological functions.

Methods

Animals. Male mice (12–16 weeks old; 25 ± 5 g body weight) were used for all experiments. All mice used in this study were on a C57BL/6J genetic background and were housed under specific pathogen-free (SPF) conditions. Animals were maintained at 22–26 °C under a 12 h:12 h light–dark cycle. NG2-DsRed mice (NG2-specific fluorescent reporter) and NG2-CreERT;Rosa26-STOP-floxed tdTomato mice (NG2-CreERT;Rosa tdTomato), and NG2-CreERT;Rosa26-STOP-floxed DTA mice (NG2-CreERT/DTA) were generated as previously described [23]. Given the well-established sex differences in muscle maintenance [26], the present study was conducted exclusively in male mice.

For depletion of $NG2^+$ cells, NG2-CreERT/DTA mice were treated with tamoxifen (Tam) (Sigma-Aldrich, St. Louis, MO, USA) at 100 mg/kg body weight. For long-term experiments, additional Tam (100 mg/kg) was given every 2 weeks to sustain depletion of $NG2^+$ cells (Fig. 1a). As controls for the $NG2^+$ cell-depletion (NG2-del) experiments, Cre-negative Rosa26-STOP-floxed DTA mice treated with Tam were used. For $NG2^+$ cell-lineage tracing, NG2-CreERT;Rosa tomato mice were treated with Tam at 10 mg/kg body weight once daily for 5 consecutive days to label $NG2^+$ cells and their descendants. Tam-treated Cre-negative littermates were used as controls.

Assessment of kyphosis. Kyphosis progression was assessed according to a previously established method for dystrophic mice [27]. Mice were euthanized under isoflurane (1.5–2.5%) anesthesia and subjected to whole-body X-ray imaging using a medical radiography system (BV Vectra; Philips). The kyphosis index (KI) was calculated by drawing a line (AB) from the caudal

edge of the last cervical vertebra to the caudal edge of the sixth lumbar vertebra (typically corresponding to the cranial border of the iliac wing), and dividing the length of AB by the maximal perpendicular distance (CD) from the dorsal edge of the vertebra at the point of greatest curvature to line AB (Fig. 1c).

Histological and immune-histological analyses. Mice were euthanized under isoflurane anesthesia, followed perfusion via heart with phosphate buffered saline (PBS), and 2% paraformaldehyde (PFA)/PBS. The harvested lung tissues were immersed in 4% PFA/PBS, and processed for paraffin embedding. Serial sections (4-5 μm) were prepared and stained with hematoxylin and eosin (H&E).

For muscle tissues, PFA-fixed samples were subsequently cryoprotected by sucrose immersion, embedded in O.C.T. compound, and stored at -80 °C until sectioning. For immunostaining studies, transverse cryosections (10-μm) were fixed in acetone for 5 min at -30 °C and air-dried. Sections were incubated for 60 min in blocking buffer (1% bovine serum albumin in PBS containing 0.3% Triton X-100). Myofiber types were identified using anti-myosin heavy chain (MyHC) antibodies. To delineate the myofiber perimeter, sections were stained with an anti-laminin antibody. Bound primary antibody was visualized with Alexa Fluorescence-conjugated anti-IgG secondary antibody. Nuclei were counterstained with DAPI (H-1200; Vector Laboratories). Images were obtained using a fluorescence microscope (BZ-X710; Keyence). The antibodies used in this study are described in Supplemental material. Histological and morphometric analyses were independently performed by two investigators who were blinded to the genotype of the animals.

Fluorescence images were analyzed using Fiji (ImageJ; ver. 2.16.0/1.54p) with the Cross-sectional Analyzer plugin. Myofiber boundaries were defined based on laminin staining, and cross section area (CSA) was quantified semi-automatically. CSA measurements were conducted in four mice per group, and ≥70 myofibers per mouse were analyzed. For morphological analysis for the neuromuscular junction (NMJ), the post-synapse (clusters of acetylcholine receptors, AChRs) was visualized by α-bungarotoixn staining. NMJ morphology was evaluated in four microscopic fields per mouse, and the proportion of morphologically abnormal NMJs, defined as shrunken or fragmented structures, was quantified (Fig. 8b).

Quantification of capillary and PC densities in muscles. For estimation of functional capillaries, NG2-DsRed mice were anesthetized and injected via the tail vein with 300 μL of FITC- or rhodamine-labeled *Griffonia simplicifolia* lectin (500 μg/mL in PBS; Vector Laboratories) as described previously [28]. Laminin staining was used to define myofiber boundaries.

For 3D-imaging assessment, fixed longitudinal sections (50 μm) were cleared with RapiClear 1.47 (SunJin Lab), and imaged with a confocal microscope (LSM900; Carl Zeiss). Serial optical sections (2-μm step) were z-stacked and rendered into 3D projections using ZEN blue, BZ-X Analyzer, and ImageJ. Capillaries and NG2-DsRed^{+} cells were visualized by lectin fluorescence and intrinsic DsRed fluorescence, respectively. Perivascular NG2-DsRed^{+} cells in contact with the lectin-labeled microvessels were classified as PCs for imaging-based quantification. Four imaging from distinct regions were analyzed for each mouse, and the measurements were averaged to obtain a single value per mouse. Their densities were quantified as fluorescence signal intensity per unit area (mm^2) or per myofiber.

Quantitative real-time (RT-PCR). Total RNA was isolated from tissues using TRIzol™ reagent (Thermo Fisher Scientific). cDNA was synthesized using the iScript™ cDNA Synthesis Kit (Bio-Rad). Real-time quantitative RT-PCR was performed on a LightCycler® 480 System (Roche) using TaqMan™ Gene Expression Master Mix (Thermo Fisher Scientific). Relative mRNA expression levels were calculated using the comparative threshold cycle (ΔΔCt) method with Gapdh as the internal control. The primer sequences used for PCR are provided in Supplemental material.

Gene microarray analysis. At 1 month after induction of NG2^{+} cells depletion (NG2-del), the digastric muscles were dissected, snap-frozen in liquid nitrogen, and stored at −80°C until analysis. Tam-treated Cre-negative Rosa26-STOP-floxed DTA mice (Cre$^{-/-}$DTA) were used as controls. Total RNA obtained from the digastric muscles of seven mice was pooled within each group to generate one control and one NG2-del samples. Thus, microarray analysis was performed using one pooled sample per group, without independent biological replication at the array level. Microarray analysis was performed using the 3D Gene Mouse Oligo Chip 24K (Toray Industries Inc., Tokyo, Japan), as previously described [22, 23]. Signal intensities were normalized by global normalization (median Cy3/Cy5 ratio = 1). Signals exceeding the background mean plus two standard deviations were considered valid. Because only one pooled sample per group was analyzed, biological variance between individual mice could not be estimated.

For Gene Ontology (GO) enrichment analysis, genes were retained if both Flag Cy3 and Flag Cy5 were classified as “OK” and the mean normalized signal intensity, calculated as (normalized Cy3 intensity + normalized Cy5 intensity)/2, was ≥50. Among these genes, those with a NG2-del /control expression ratio ≥2.0 were classified as candidates showing increased expression, whereas those with a ratio ≤0.5 were classified as candidates showing decreased

expression. The two candidate gene sets were separately subjected to GO enrichment analysis using Metascape.

Statistical analysis. Data are presented as mean ± standard error of the mean (SEM) unless otherwise noted. Sample sizes (n) are provided in the figure legends. Unless otherwise indicated, Two-group comparisons were performed using an unpaired Student's t-test. Survival analysis included mice prospectively assigned to an observation period of at least 4 months. Mice that remained alive at the end of their scheduled observation period were censored at that time point. Survival curves were estimated using the Kaplan–Meier method and compared using the log-rank test. Longitudinal body-weight data from 0.5 to 3 months after induction of $NG2^+$ cells depletion were analyzed using a mixed-effects model fitted by restricted maximum likelihood (REML). Šídák's multiple-comparisons test was used to compare the control and NG2-del groups at each time point. The pretreatment time point was excluded from the mixed-effects analysis because all pretreatment values were fixed at 1 by normalization.

All analyses were performed using Prism software (version 10.6.1; GraphPad Software). A P value < 0.05 was considered statistically significant.

Results

1. Repeated depletion of $NG2^+$ cells leads to delayed-onset systemic deterioration with body weight loss and increased mortality. To ablate $NG2^+$ cells *in vivo*, tamoxifen (Tam) treatment was administered to NG2-CreERT2/DTA mice every 2 weeks. Tam-treatment was administered to mice for up to four months (Fig. 1a). No apparent changes in general condition were observed during the first 1–2 months. Interestingly, Tam-treatment for more than three months resulted in sudden decrease in body weight and increased mortality, with most mice dying after three months of treatment (Fig. 1b, c).

2. Kyphosis and respiratory abnormalities are associated with the observed mortality in these mice. Three months after Tam-treatment, mice exhibited marked body weight loss accompanied by overt spinal deformities (Fig. 1d). X-ray imaging revealed progressive kyphotic curvature of the spine in NG2-del group and quantitative evaluation confirmed this deformity as a significant reduction in the kyphosis index (KI) compared with controls (Fig. 1d).

Severe thoracic deformity was accompanied by respiratory dysfunction. High-pitched vocalization, wheezing was frequently observed in these mice (Supplemental Movie). In addition, histological examination of lung tissue revealed the presence of foreign material, such as hair, within the air way, accompanied by inflammatory changes (Fig. 2a). Marked upregulation of inflammatory cytokines, IL1β, IL6 and TNFα was observed in the lung tissues (Fig. 2b).

Collectively, these findings are consistent with pathology related to aspiration pneumonia, although swallowing function was not directly assessed.

3. NG2$^+$ cell-depletion induces muscle atrophy in posture- and swallowing-related muscles. We previously reported that one or two rounds of induced NG2$^+$ cell-depletion led to atrophy of slow-twitch muscles such as the soleus, in the hindlimbs [23]. In the present study, repeated induction of cell deletion induced atrophy across muscle groups throughout the body under normal homeostatic conditions. Notably, in accordance with the systemic phenotypic changes, including spinal deformities and respiratory dysfunction, marked atrophy was observed in paraspinal muscles as well as in swallowing-related pharyngeal muscle groups (Fig. 3, 4).

Among the paraspinal muscle groups, atrophy was observed selectively in the erector spinae muscles (ESM) involved in postural control (Fig. 3a). Myofiber size was reduced, accompanied by mild infiltration of interstitial cells, while centrally nucleated regenerating myofibers were rarely observed (Fig. 3b). In the pharyngeal region, marked atrophy was noted in the suprahyoid muscles, especially the digastric muscle (DIG) (Fig. 4a, b). Myofiber atrophy in these muscle groups was also observed as early as one month, with further decreased at 2 months after Tam-treatment (Fig 4c). This was accompanied by a leftward shift in myofiber cross section area (CSA) distribution, with an increased proportion of small myofibers (Fig 4d). Together, these data indicate that muscle atrophy following NG2$^+$ cell depletion occurs, and in a time-dependent manner in muscle groups involved in posture and swallowing.

4. NG2$^+$ cells contribute to muscle regeneration in the dorsal trunk and pharynx. Using NG2$^+$ cell-lineage tracing mice (NG2CreERT; Rosa26-tdTomato), we assessed whether muscles that undergo atrophy following NG2$^+$ cell-depletion are identical to those derived from NG2$^+$ cells. In the erector spinae muscle (ESM), tdTomato-expressing muscle fibers were detected particularly in the deep medial side (medial ESM) that underwent atrophy following NG2$^+$ cell depletion, but not in lateral side of paraspinal muscles (lateral ESM) (Fig. 5a). Immunohistochemical analysis demonstrated that medial ESM consisted predominantly of type I (slow-twitch) and type IIA (fast-twitch) fibers, whereas lateral ESM were composed almost exclusively of type IIA and type IIB fast-twitch fibers and lacked type I fibers (Fig. 5b, Fig. S1). Consisting with the previous findings [23], these findings indicate that NG2$^+$ cell-depletion preferentially induces slow-twitch muscle atrophy in paraspinal muscles.

In the pharyngeal region, tdTomato-expressing fibers were observed across various subregions, including tongue, oropharynx, hypopharynx and DIG (Fig. 6a). Muscles in pharynx including DIG were composed predominantly of type IIA/IIB fast-twitch fibers and lacked type I fibers; accordingly, most tdTomato-expressing fibers were type II fibers (Fig. 6b, Fig. S1).

Therefore, unlike somite-derived muscles including hindlimb and ESM, $NG2^+$ cell-depletion induced atrophy in fast-twitch muscle fibers in the pharyngeal muscle groups.

tdTomato expression kinetics were assessed at multiple time points following Tam-treatment (Fig. S2). In the hindlimb soleus but not gastrocnemius, TdTomato-expressing myofibers were detected within one week and reached a maximum of approximately 80% within one month as described previously [23]. tdTomato-expressing fibers appeared in DIG at a rate comparable to that of the soleus, despite its fast-twitch fiber dominance (Fig. S2).

5. Dependency on $NG2^+$ cells in muscular maintenance is associated with microvascular density. To test whether the contribution of $NG2^+$ cells to muscular maintenance depends on the local microenvironment in a muscle-specific manner, we quantified functional microvessels by lectin labeling and assessed $NG2^+$ cells abundance using NG2-DsRed mice in the soleus, gastrocnemius, the erector spinae and the pharyngeal muscles.

It is well recognized that muscles enriched in slow-twitch fibers generally exhibit greater capillary supply, whereas fast-twitch fibers tend to be less vascularized [29, 30]. Consistently, confocal 3D-imaging of cleared muscle tissues demonstrated that density of microvessels was indeed higher in the slow-twitch dominant soleus and medial-ESM, and lower in the fast-twitch dominant gastrocnemius and lateral-ESM (Fig. 7). $NG2^+$ cells were closely associated with the microvascular network (Fig. 7a). Among these cells, those adjacent to microvessels were identified as PCs, and accordingly, PCs were more abundant in slow-twitch muscles, which had a higher microvessel density (Fig. 7b). Unexpectedly, the pharyngeal muscle groups including DIG, despite being composed predominantly of fast-twitch fibers displayed a high density of microvasculature and PCs comparable to that of the soleus (Fig. 7). Collectively, these selective muscle atrophy after $NG2^+$ cell-depletion and the kinetics of $NG2^+$ cell-lineage-derived tdTomato-expressing myofiber appearance can be explained by muscle-specific local environments, including the degree of vascularization than by a simplistic “slow vs. fast” muscle type dichotomy.

6. $NG2^+$ cell depletion induces morphological abnormalities in the neuromuscular junction. Maintenance of skeletal muscle depends not only on myofibers themselves, but also on intact neural innervation, particularly neuromuscular junction (NMJ) [31, 32]. Terminal Schwann cells (tSCs) play essential roles in NMJ maintenance and remodeling, and $NG2^+$ peri-synaptic glia/PC-like cells have recently been recognized as components of tSCs [33, 34]. We therefore examined the impact of $NG2^+$ cell depletion on NMJ in skeletal muscle.

To assess NMJ morphology in skeletal muscle, cluster of nicotinic acetylcholine receptors (nAChR) was visualized by α-bungarotoxin staining (Fig. 8a). $NG2^+$ cell-depletion

reduced the proportion of morphologically intact NMJs and increased structurally abnormal fragmented NMJs, indicative of impaired NMJ stability (Fig. 8b).

7. Gene expression profile in atrophic pharyngeal muscles following NG2$^+$ cells depletion. To elucidate the mechanisms underlying pharyngeal muscle atrophy induced by NG2$^+$ cell-depletion, gene expression profiles of these muscles were analyzed using the digastric muscle, DIG. After 1 month of NG2$^+$ cells depletion, gene expression in the DIG was compared between control and NG2-del groups by quantitative PCR (qPCR).

NG2 gene expression was reduced by 50% in NG2-del group. Under the present condition, Pax7 gene expression showed a modest decrease of approximately 20% (Fig. 9a). Pax7$^+$ SCs play a critical role in the regeneration of *de novo* muscular fiber regeneration after muscle injury [8, 10]. Among myogenic regulators particularly involved in the early phase of muscle regeneration, *Myf5* and *MyoD* exhibited a tendency toward decreased expression. In contrast, expression of the late-stage myogenic regulator *Myogenin* was significantly upregulated, suggesting activation of a differentiation and/or muscle repair process (Fig. 9a). Expression of the embryonic isoform *Myh3* and the slow-twitch isoform *Myh7* was significantly increased in the DIG of NG2-del mice, whereas the first-twitch isoform *Myh2* and *Mhy4* expression were not altered (Fig. 9a).

Furthermore, comprehensive microarray analysis demonstrated broad downregulation of sarcomeric and muscle structural gene modules, accompanied by induction of an immature or developmental-like transcriptional program (Fig. 9b). Gene Ontology enrichment analysis identified gene sets related to tissue remodeling, inflammation, and fibrosis, potentially reflecting secondary tissue responses following NG2$^+$ cells depletion (Fig. 9b). Notably, ectopic expression of cardiomyocyte-associated and embryonic myogenic transcripts such as *Tnnt2* and *Myl4* were detected (Table 1). This pattern is consistent with the qPCR-detected increase in *Myh3* (Fig. 9a), suggesting incomplete myofiber maturation at an intermediate stage of the muscle regenerative process. In NG2-del muscles, neural regeneration-related genes were altered, particularly downregulation of genes associated with NMJ formation and maintenance. Expression of *Agrin* and *Neuregulin*, presynaptic factors that promote NMJ assembly, was reduced, together with *MuSK* and *Rapsn*, which mediate AchR clustering, and the synapse-associated genes such as *Col13a* and *Lamb2*. In contrast, canonical genes associated with hypoxic responses, angiogenesis showed no significant changes (Table 1).

Discussion

A key finding of this study is that $NG2^+$ cell dependency across skeletal muscle groups throughout the body is determined not by slow-twitch classification *per se* but instead depends on the characteristic of high microvascular density. It is well recognized that skeletal muscle is classified into slow- and fast-twitch types according to myosin heavy chain (MyHC) expression patterns, with slow-twitch muscles characterized by higher microvascular density and distinct metabolic properties compared with fast-twitch muscles, *i.e.* oxidative and glycolytic, respectively [29, 35]. This fiber type–independent phenomenon was predominantly observed in the pharyngeal muscle groups, including DIG. Head/neck, pharyngeal skeletal muscles are developmentally distinct from somite-derived muscles, including limb and trunk muscles and differ substantially in their structural and functional properties [36, 37]. Notably, the fast-twitch fiber–dominant DIG exhibited $NG2^+$ cell dependency and unexpectedly high microvascular density comparable to somite-derived slow-twitch muscles, supporting a model in which $NG2^+$ cell-mediated muscular maintenance depends on the vascular microenvironment rather than fiber type.

A second major finding is that $NG2^+$ cell depletion causes atrophy in trunk and pharyngeal muscles and is accompanied by respiratory abnormalities and aspiration pneumonia-like lung pathology. Because swallowing function was not directly measured, a causal sequence from pharyngeal muscle atrophy to dysphagia, aspiration, and death cannot be established from the present data. Primary myogenic stem cells, SCs contribute to postnatal muscle growth and the maintenance of adult skeletal muscle homeostasis by supplying new myonuclei. The cellular properties of SCs, as well as their homeostatic demand within muscle fibers, differ according to the location of the muscle [38]. In pharyngeal muscles, SCs exhibit high proliferative in steady condition, reflecting a high level of myonuclear turnover for muscle maintenance [14]. SC depletion did not induce hindlimb muscle atrophy [12], but pharyngeal muscles exhibited a tendency toward atrophy [14]. Nevertheless, no overt severe systemic abnormalities have been reported in association with SC depletion.

Mechanisms underlying $NG2^+$ cell depletion-induced muscle atrophy. A subset of PC population has been reported to function as myogenic stem cells involved in muscle regeneration and maintenance [19-22]. Here, we demonstrate that $NG2^+$ cells contribute to myonuclear replenishment essential for muscle maintenance *in vivo*, using $NG2^+$ cell-lineage tracing and $NG2^+$ cell-depletion mouse models. Muscular fiber types are known to dynamically transition during muscle maturation process, as reflected by changes in MyHC isoform expression [39].

Microarray analysis revealed broad suppression of muscle structural/contractile-related genes together with induction of immature/development-like transcriptional, and inflammatory/fibrotic remodeling-associated programs (Fig. 9, Table1). These results are consistent with the possibility of compensatory remodeling or transition process from immature regenerating muscle fibers to functionally mature muscle fibers in the fast-twitch-dominant DIG following $NG2^+$ cells depletion. Given that PCs are essential for maintaining microvascular structure and function [18], $NG2^+$ cell-depletion may result in circulatory dysfunction and subsequent secondary muscle impairment, *i.e.* ischemic damage. However, the absence of centrally nucleated fibers indicates that muscle fibers are not undergoing extensive damage and that *de novo* muscle regeneration is not occurring. In addition, analysis of gene expression profiles in atrophied muscles following $NG2^+$ cells depletion revealed no evident signatures of ischemia or compensatory angiogenic activation.

$NG2^+$ cell-depletion induced abnormalities in NMJ morphology in atrophied muscles (Fig. 8), suggesting that neural transmission systems within these muscles are impaired. The terminal Schwann cells (tSCs) are specialized non-myelinating synaptic glia at the NMJ, that participate in synapse maintenance, and repair. tSC depletion causes axonal retraction and destabilization of the NMJ, both structurally and functionally [40]. Because NG2 is expressed not only in PCs but also expressed in tSCs associated with the NMJ [33], the NMJ abnormalities observed in our model may result from depletion of $NG2^+$ cells functioning as tSCs. Thus, the muscle atrophy induced by $NG2^+$ cell-depletion in the present study might be mediated, at least in part, by NMJ dysfunction-associated muscle wasting. Whether PCs and tSCs represent distinct cellular populations remains unclear. Notably, subsets of PCs exhibit neural stem cell-like properties and differentiate into Schwann cells in response to nerve injury, contributing to nerve regeneration [41, 42]. Because NMJ are closely associated with a dense microvascular network [43], the local microvascular niche may support NMJ integrity through neurogenic or Schwann cell–competent PCs.

The inter-myofiber microenvironment, consisting of microvasculature and mesenchymal cells, including fibro/adipogenic progenitors (FAPs), is known to function as a niche for satellite cells (SCs) maintenance [16, 44-46]. Microvascular endothelial cells (ECs) and PCs can regulate SC activation states, *i.e.* quiescence and proliferation through vascular niche factors such as IGF1 and Angpt1, and the physical distance between microvessels and SCs is considered to be a key determinant of this regulatory process [15, 47]. In the present study, atrophic skeletal muscle from NG2-del mice exhibited reduced Pax7 gene expression accompanied by a decrease in NG2 gene expression (Fig. 9). Therefore, the muscle atrophy following $NG2^+$ cells depletion may be

attributable to dysfunction of the microenvironmental niche involved in the maintenance of SCs. However, it remains to be determined whether SC function, in addition to cell number, is affected by $NG2^+$ cell-depletion. In addition, further studies are required to clarify the role of PCs in the local microvascular environment and to elucidate the interactions between SCs and microvascular PCs and ECs.

Delayed onset of $NG2^+$ cell depletion-induced effects. To account for the delayed onset of life-threatening phenotypes emerged after 3 months following repeated $NG2^+$ cell-depletion, we considered the possibility of compensatory replacement or replenishment of PCs. Berthiaume *et al.* showed that *in vivo* optical ablation of individual microvascular PCs in a cranial window leads to PC replacement within days, although the source of the replenishing PCs remains unknown [25]. In wound healing sites, $NG2^+$ PDGFRβ^+PCs covering newly formed vessels are replenished through recruitment and phenotypic conversion of $NG2^-$ PDGFR β^+ mesenchymal cells [24]. It has also been reported that, via Notch signaling, dynamic phenotypic transitions from SCs to PCs contribute to vascular network formation [48]. Therefore, $NG2^+$ cell-depletion does not immediately cause lethal homeostatic failure; rather, compensatory mechanisms are transiently maintained until their capacity is ultimately exceeded. The mechanisms underlying PC replenishment that maintain the microenvironmental niche for skeletal muscle homeostasis, including the cellular sources and molecular determinants in response to PC loss, remain to be elucidated.

Clinical implications of these findings. Pneumonia, including aspiration pneumonia, represents a leading cause of mortality in aging societies and is closely associated with sarcopenia [49-51]. Sarcopenia is a multifactorial syndrome, with factors beyond aging, such as malnutrition, physical inactivity, and underlying diseases including cancer and diabetes mellitus (DM), contributing to its onset and progression [4]. While sarcopenia has been characterized by preferential atrophy of fast-twitch fibers, muscle vulnerability across different anatomical regions is not fully explained by differences in fiber type or levels of physical activity [52]. For instance, age-related muscle atrophy preferentially affects hindlimbs over forelimbs in both humans and quadrupedal animals, independent of loading. In cancer cachexia, atrophy is observed in hindlimb but not masticatory muscles, despite both being predominantly fast-twitch fibers [53]. Microvascular dysfunction, including PC loss, is recognized as a fundamental pathological feature of DM [54]. Notably, patients with DM and obesity-associated metabolic disorders exhibit preferential atrophy of capillary-rich slow-twitch fibers [55, 56].

SCs exhibit marked heterogeneity, and regional differences in muscle vulnerability may partly reflect site-specific variations in SC properties [38]. However, the role of SCs in sarcopenia

remains debated [12, 13]. Recent studies have demonstrated that abnormalities in NMJ innervation, as well as dysfunction of terminal Schwann cells (tSCs), which are essential for NMJ maintenance, contribute to the pathogenesis of sarcopenia [31, 32]. Increasing evidence indicates that muscle regeneration and maintenance are regulated by integrated mechanisms involving myogenic SCs, tSCs, and the surrounding microenvironmental niche. [52]. Thus, elucidating the role of the microvasculature-inclusive niche will be critical for understanding sarcopenia.

Conclusion

Our findings indicate that $NG2^+$ cells contribute to the maintenance of skeletal muscles across anatomical regions, including postural and pharyngeal muscles. Muscle vulnerability following repeated $NG2^+$ cell-depletion was associated with a capillary-rich local microenvironment and did not show a consistent relationship with fiber type *per se*. Depletion was also accompanied by neuromuscular junction abnormalities, respiratory pathology, and increased mortality. However, NG2-based depletion targets multiple cell populations, so the respective contributions of PCs and tSCs remain unresolved. Moreover, neither swallowing dysfunction nor a causal link between muscle atrophy and mortality was directly established. Further studies are needed to identify the responsible cell populations and determine how they support muscle and systemic homeostasis.

List of abbreviations

NG2 Neuroglial 2 proteoglycan, PCs Pericytes, ECs Endothelial cells, SCs Satellite cells, MSCs Mesenchymal stem cells, NSCs Neural stem cells, FAPs Fibro-adipogenic progenitors, tSCs Terminal Schwann cells, NMJ Neuro-muscular junction, PDGFR Platelet-derived growth factor receptor, AChRs Acetylcholine receptors, Tam tamoxifen, DTA Diphtheria toxin A, Pax paired box, MyHC Myosin heavy chain, Myf Myogenic factor, Myh Myosin heavy chain, MyoD Myogenic differentiation, DM Diabetes mellitus,

Declarations

Ethics approval and consent to participate; All animal experiments were approved by the Animal Care and Use Committee of Asahikawa Medical University (approval number, R8-104, R8-106) and were conducted in accordance with the institutional guidelines.

Consent for publication; not applicable

Availability of data and materials; The datasets used and analyzed during the current study are available from the corresponding author on reasonable request.

Competing interests; The authors declared that no conflict of interest exists.

Funding support; This work was supported by JSPS KAKENHI Grants 22K07018 (to JK), 24K19412(to TT), 23K10474 (to KN) and 24K23200 (to YW).

Authors' contributions; HS, TT, JK conceived and designed the research, conducted experiments, acquired and analyzed the data, and wrote the initial draft of the manuscript. HS, TT, KN, YW, HS, YK, YI, YS, ST, performed experiments and contributed to data acquisition and curation. KN, YM, TY, MT contributed to study design, data interpretation, and critical revision of the manuscript. All authors provided input on the writing and approved the final version of the manuscript.

Acknowledgements; We thank A. Oda, S. Takahashi, Y. Horikawa, and A. Kawamura for laboratory assistance, and K. Segawa for secretarial assistance

References

1. Yin H, Price F, Rudnicki MA. Satellite cells and the muscle stem cell niche. Physiol Rev. 2013;93:23-67.
2. Severinsen MCK, Pedersen BK. Muscle-Organ Crosstalk: The Emerging Roles of Myokines. Endocr Rev. 2020;41:594-609.
3. Cruz-Jentoft AJ, Bahat G, Bauer J, Boirie Y, Bruyere O, Cederholm T, et al. Sarcopenia: revised European consensus on definition and diagnosis. Age Ageing. 2019;48:16-31.
4. Huo F, Liu Q, Liu H. Contribution of muscle satellite cells to sarcopenia. Front Physiol. 2022;13:892749.
5. Gundersen K. Muscle memory and a new cellular model for muscle atrophy and hypertrophy. J Exp Biol. 2016;219:235-42.
6. Murach KA, Fry CS, Kirby TJ, Jackson JR, Lee JD, White SH, et al. Starring or Supporting Role? Satellite Cells and Skeletal Muscle Fiber Size Regulation. Physiology (Bethesda). 2018;33:26-38.
7. Charge SB, Rudnicki MA. Cellular and molecular regulation of muscle regeneration. Physiol Rev. 2004;84:209-38.
8. Wang YX, Rudnicki MA. Satellite cells, the engines of muscle repair. Nat Rev Mol Cell Biol. 2011;13:127-33.
9. Sambasivan R, Yao R, Kissenpfennig A, Van Wittenberghe L, Paldi A, Gayraud-Morel B, et al. Pax7-expressing satellite cells are indispensable for adult skeletal muscle regeneration. Development. 2011;138:3647-56.
10. Lepper C, Partridge TA, Fan CM. An absolute requirement for Pax7-positive satellite cells in acute injury-induced skeletal muscle regeneration. Development. 2011;138:3639-46.
11. Roth SM, Martel GF, Ivey FM, Lemmer JT, Metter EJ, Hurley BF, et al. Skeletal muscle satellite cell populations in healthy young and older men and women. Anat Rec. 2000;260:351-8.
12. Fry CS, Lee JD, Mula J, Kirby TJ, Jackson JR, Liu F, et al. Inducible depletion of satellite cells in adult, sedentary mice impairs muscle regenerative capacity without affecting sarcopenia. Nat Med. 2015;21:76-80.
13. Keefe AC, Lawson JA, Flygare SD, Fox ZD, Colasanto MP, Mathew SJ, et al. Muscle stem cells contribute to myofibres in sedentary adult mice. Nat Commun. 2015;6:7087.
14. Randolph ME, Phillips BL, Choo HJ, Vest KE, Vera Y, Pavlath GK. Pharyngeal Satellite Cells Undergo Myogenesis Under Basal Conditions and Are Required for Pharyngeal Muscle Maintenance. Stem Cells. 2015;33:3581-95.
15. Verma M, Asakura Y, Murakonda BSR, Pengo T, Latroche C, Chazaud B, et al. Muscle Satellite Cell Cross-Talk with a Vascular Niche Maintains Quiescence via VEGF and Notch Signaling. Cell Stem Cell. 2018;23:530-43 e9.
16. Wosczyna MN, Konishi CT, Perez Carbajal EE, Wang TT, Walsh RA, Gan Q, et al. Mesenchymal Stromal Cells Are Required for Regeneration and Homeostatic Maintenance of Skeletal Muscle. Cell Rep. 2019;27:2029-35 e5.
17. Henrot P, Blervaque L, Dupin I, Zysman M, Esteves P, Gouzi F, et al. Cellular interplay in skeletal muscle regeneration and wasting: insights from animal models. J Cachexia Sarcopenia Muscle. 2023;14:745-57.

18. Armulik A, Genove G, Betsholtz C. Pericytes: developmental, physiological, and pathological perspectives, problems, and promises. Dev Cell. 2011;21:193-215.
19. Dellavalle A, Sampaolesi M, Tonlorenzi R, Tagliafico E, Sacchetti B, Perani L, et al. Pericytes of human skeletal muscle are myogenic precursors distinct from satellite cells. Nat Cell Biol. 2007;9:255-67.
20. Dellavalle A, Maroli G, Covarello D, Azzoni E, Innocenzi A, Perani L, et al. Pericytes resident in postnatal skeletal muscle differentiate into muscle fibres and generate satellite cells. Nat Commun. 2011;2:499.
21. Birbrair A, Zhang T, Wang ZM, Messi ML, Enikolopov GN, Mintz A, et al. Skeletal muscle pericyte subtypes differ in their differentiation potential. Stem Cell Res. 2013;10:67-84.
22. Kano K, Horiuchi K, Yoshida Y, Hayasaka T, Kabara M, Tomita Y, et al. EphA7(+) perivascular cells as myogenic and angiogenic precursors improving skeletal muscle regeneration in a muscular dystrophic mouse model. Stem Cell Res. 2020;47:101914.
23. Tatsukawa T, Kano K, Nakajima KI, Yazawa T, Eguchi R, Kabara M, et al. NG2-positive pericytes regulate homeostatic maintenance of slow-type skeletal muscle with rapid myonuclear turnover. Stem Cell Res Ther. 2023;14:205.
24. Morikawa S, Ezaki T. Phenotypic changes and possible angiogenic roles of pericytes during wound healing in the mouse skin. Histol Histopathol. 2011;26:979-95.
25. Berthiaume AA, Schmid F, Stamenkovic S, Coelho-Santos V, Nielson CD, Weber B, et al. Pericyte remodeling is deficient in the aged brain and contributes to impaired capillary flow and structure. Nat Commun. 2022;13:5912.
26. Kerr HL, Krumm K, Anderson B, Christiani A, Strait L, Li T, et al. Mouse sarcopenia model reveals sex- and age-specific differences in phenotypic and molecular characteristics. J Clin Invest. 2024;134.
27. Laws N, Hoey A. Progression of kyphosis in mdx mice. J Appl Physiol (1985). 2004;97:1970-7.
28. Minoshima A, Kabara M, Matsuki M, Yoshida Y, Kano K, Tomita Y, et al. Pericyte-Specific Ninjurin1 Deletion Attenuates Vessel Maturation and Blood Flow Recovery in Hind Limb Ischemia. Arterioscler Thromb Vasc Biol. 2018;38:2358-70.
29. Hudlicka O, Brown M, Egginton S. Angiogenesis in skeletal and cardiac muscle. Physiol Rev. 1992;72:369-417.
30. Deveci D, Marshall JM, Egginton S. Relationship between capillary angiogenesis, fiber type, and fiber size in chronic systemic hypoxia. Am J Physiol Heart Circ Physiol. 2001;281:H241-52.
31. Bao Z, Cui C, Chow SK, Qin L, Wong RMY, Cheung WH. AChRs Degeneration at NMJ in Aging-Associated Sarcopenia-A Systematic Review. Front Aging Neurosci. 2020;12:597811.
32. Iyer SR, Shah SB, Lovering RM. The Neuromuscular Junction: Roles in Aging and Neuromuscular Disease. Int J Mol Sci. 2021;22.
33. Castro R, Taetzsch T, Vaughan SK, Godbe K, Chappell J, Settlage RE, et al. Specific labeling of synaptic schwann cells reveals unique cellular and molecular features. Elife. 2020;9.
34. Guzman SD, Abu-Mahfouz A, Davis CS, Ruiz LP, Macpherson PC, Brooks SV.

Decoding muscle-resident Schwann cell dynamics during neuromuscular junction remodeling. JCI Insight. 2026;11.
35. Poole DC, Mathieu-Costello O. Relationship between fiber capillarization and mitochondrial volume density in control and trained rat soleus and plantaris muscles. Microcirculation. 1996;3:175-86.
36. Buckingham M. Skeletal muscle formation in vertebrates. Curr Opin Genet Dev. 2001;11:440-8.
37. Sambasivan R, Tajbakhsh S. Skeletal muscle stem cell birth and properties. Semin Cell Dev Biol. 2007;18:870-82.
38. Ono Y, Boldrin L, Knopp P, Morgan JE, Zammit PS. Muscle satellite cells are a functionally heterogeneous population in both somite-derived and branchiomeric muscles. Dev Biol. 2010;337:29-41.
39. Schiaffino S, Reggiani C. Fiber types in mammalian skeletal muscles. Physiol Rev. 2011;91:1447-531.
40. Reddy LV, Koirala S, Sugiura Y, Herrera AA, Ko CP. Glial cells maintain synaptic structure and function and promote development of the neuromuscular junction in vivo. Neuron. 2003;40:563-80.
41. Yoshida Y, Kabara M, Kano K, Horiuchi K, Hayasaka T, Tomita Y, et al. Capillary-resident EphA7(+) pericytes are multipotent cells with anti-ischemic effects through capillary formation. Stem Cells Transl Med. 2020;9:120-30.
42. Tomita Y, Horiuchi K, Kano K, Tatsukawa T, Matsuo R, Hayasaka T, et al. Ninjurin 1 mediates peripheral nerve regeneration through Schwann cell maturation of NG2-positive cells. Biochem Biophys Res Commun. 2019;519:462-8.
43. Pierzga JM, Segal SS. Spatial relationships between neuromuscular junctions and microvessels in hamster cremaster muscle. Microvasc Res. 1994;48:50-67.
44. Mashinchian O, Pisconti A, Le Moal E, Bentzinger CF. The Muscle Stem Cell Niche in Health and Disease. Curr Top Dev Biol. 2018;126:23-65.
45. Uezumi A, Ikemoto-Uezumi M, Zhou H, Kurosawa T, Yoshimoto Y, Nakatani M, et al. Mesenchymal Bmp3b expression maintains skeletal muscle integrity and decreases in age-related sarcopenia. J Clin Invest. 2021;131.
46. Yang C, Zhang L, Liu L, Bai L, Liu Y, Wang R, et al. Advances in vascular endothelial cell-mediated regulation of satellite cell repair and regeneration. Inflamm Regen. 2025;45:30.
47. Abou-Khalil R, Le Grand F, Pallafacchina G, Valable S, Authier FJ, Rudnicki MA, et al. Autocrine and paracrine angiopoietin 1/Tie-2 signaling promotes muscle satellite cell self-renewal. Cell Stem Cell. 2009;5:298-309.
48. Gerli MFM, Moyle LA, Benedetti S, Ferrari G, Ucuncu E, Ragazzi M, et al. Combined Notch and PDGF Signaling Enhances Migration and Expression of Stem Cell Markers while Inducing Perivascular Cell Features in Muscle Satellite Cells. Stem Cell Reports. 2019;12:461-73.
49. Fujishima I, Fujiu-Kurachi M, Arai H, Hyodo M, Kagaya H, Maeda K, et al. Sarcopenia and dysphagia: Position paper by four professional organizations. Geriatr Gerontol Int. 2019;19:91-7.
50. Okazaki T, Ebihara S, Mori T, Izumi S, Ebihara T. Association between sarcopenia and

pneumonia in older people. Geriatr Gerontol Int. 2020;20:7-13.
51. de Sire A, Ferrillo M, Lippi L, Agostini F, de Sire R, Ferrara PE, et al. Sarcopenic Dysphagia, Malnutrition, and Oral Frailty in Elderly: A Comprehensive Review. Nutrients. 2022;14.
52. Sousa-Victor P, Garcia-Prat L, Munoz-Canoves P. Control of satellite cell function in muscle regeneration and its disruption in ageing. Nat Rev Mol Cell Biol. 2022;23:204-26.
53. Yoshioka K, Kitajima Y, Seko D, Tsuchiya Y, Ono Y. The body region specificity in murine models of muscle regeneration and atrophy. Acta Physiol (Oxf). 2021;231:e13553.
54. Horton WB, Barrett EJ. Microvascular Dysfunction in Diabetes Mellitus and Cardiometabolic Disease. Endocr Rev. 2021;42:29-55.
55. Frankenberg NT, Mason SA, Wadley GD, Murphy RM. Skeletal muscle cell-specific differences in type 2 diabetes. Cell Mol Life Sci. 2022;79:256.
56. Serrano N, Hyatt JK, Houmard JA, Murgia M, Katsanos CS. Muscle fiber phenotype: a culprit of abnormal metabolism and function in skeletal muscle of humans with obesity. Am J Physiol Endocrinol Metab. 2023;325:E723-E33.

Figures and Figure legends

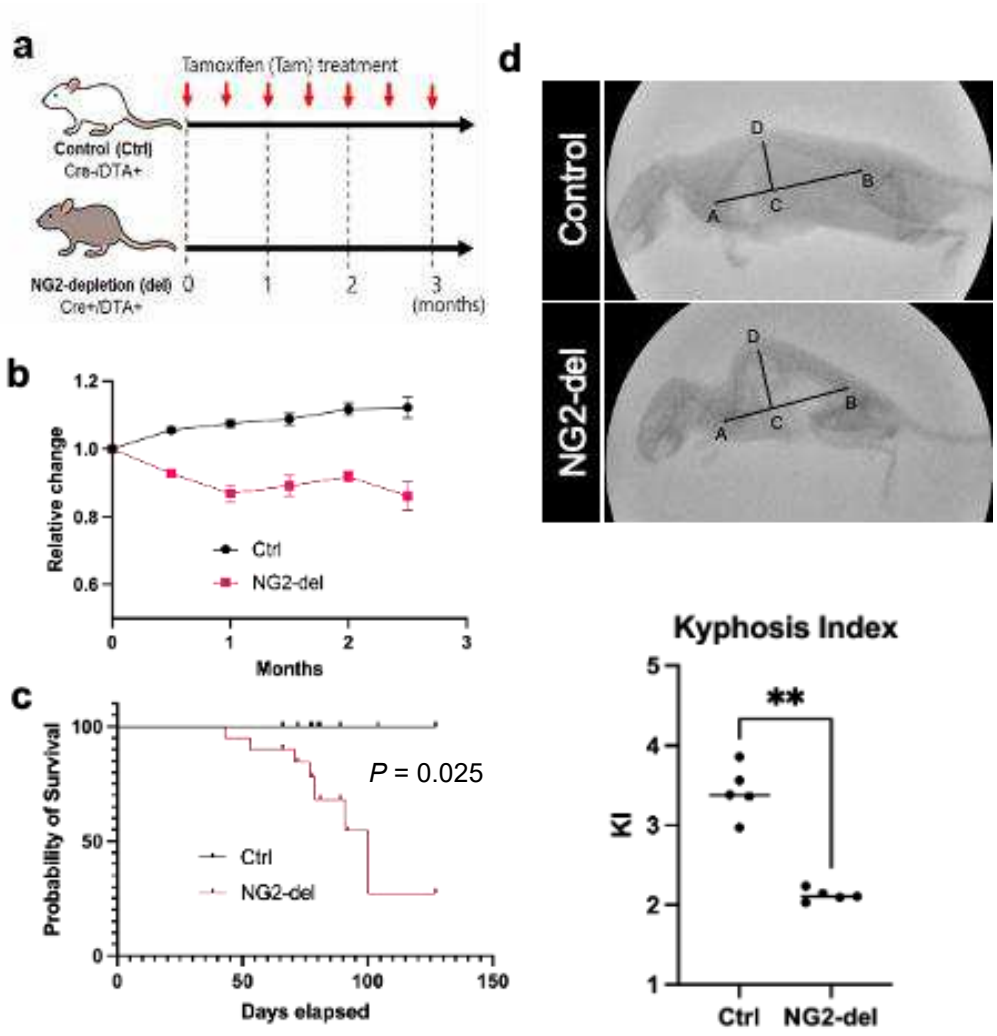


Fig. 1 Systemic phenotypic deterioration and kyphosis following NG2$^+$ cell depletion

a. For NG2$^+$ cell depletion, NG2-CreERT/DTA mice were treated with tamoxifen (Tam) every 2 weeks. Tam-treated Cre-negative Rosa26-STOP-floxed DTA mice as control (Ctrl). **b.** Time course of body weight after NG2$^+$ cell depletion (NG2-del). The values are presented as the means ± SEM (n=21-23), $^{**}P < 0.01$. **c.** Kaplan–Meier survival analysis of NG2-del and Ctrl mice. **d.** Whole-body X-ray images of NG2-del and control mice at 3 months after Tam-treatment. Quantification of kyphosis was estimated by kyphosis index (KI). Data are presented as mean ± SEM (n=5), $^{**}P < 0.01$

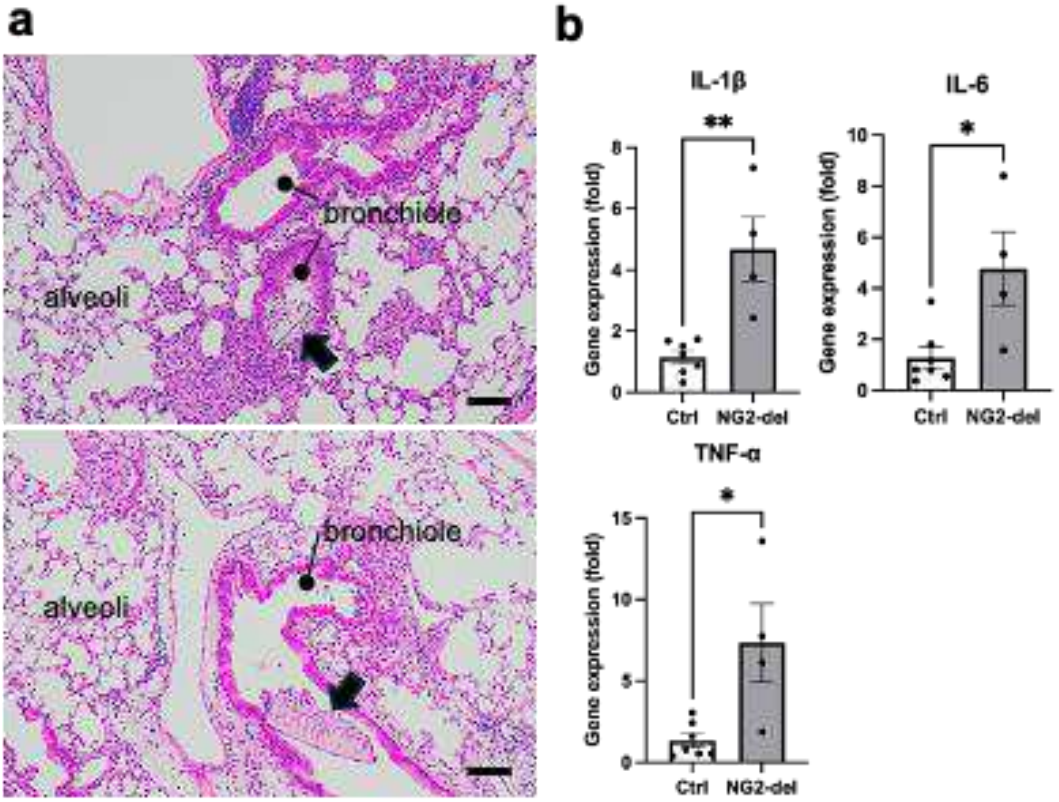


Fig. 2 Aspiration pneumonia–like lesions after NG2$^+$ cell depletion

a. Representative hematoxylin and eosin (H&E) -stained lung sections from NG2$^+$ cell-depletion mice (NG2-del). Intraluminal foreign material within the airway (*arrow*), inflammatory cell infiltration, and disruption of alveolar architecture were observed, consistent with aspiration pneumonia–like pathology. These lesions were not observed in control mice (Ctrl). Scale bar=100 μm. **b.** Relative gene expression of inflammatory cytokines (IL-1β, IL-6, and TNF-α) in lung tissue as assessed by real-time quantitative RT-PCR. Expression of these cytokines was significantly increased in NG2-del. Data are presented as mean ± SEM (n=4~7), **P* < 0.05, ***P* < 0.01

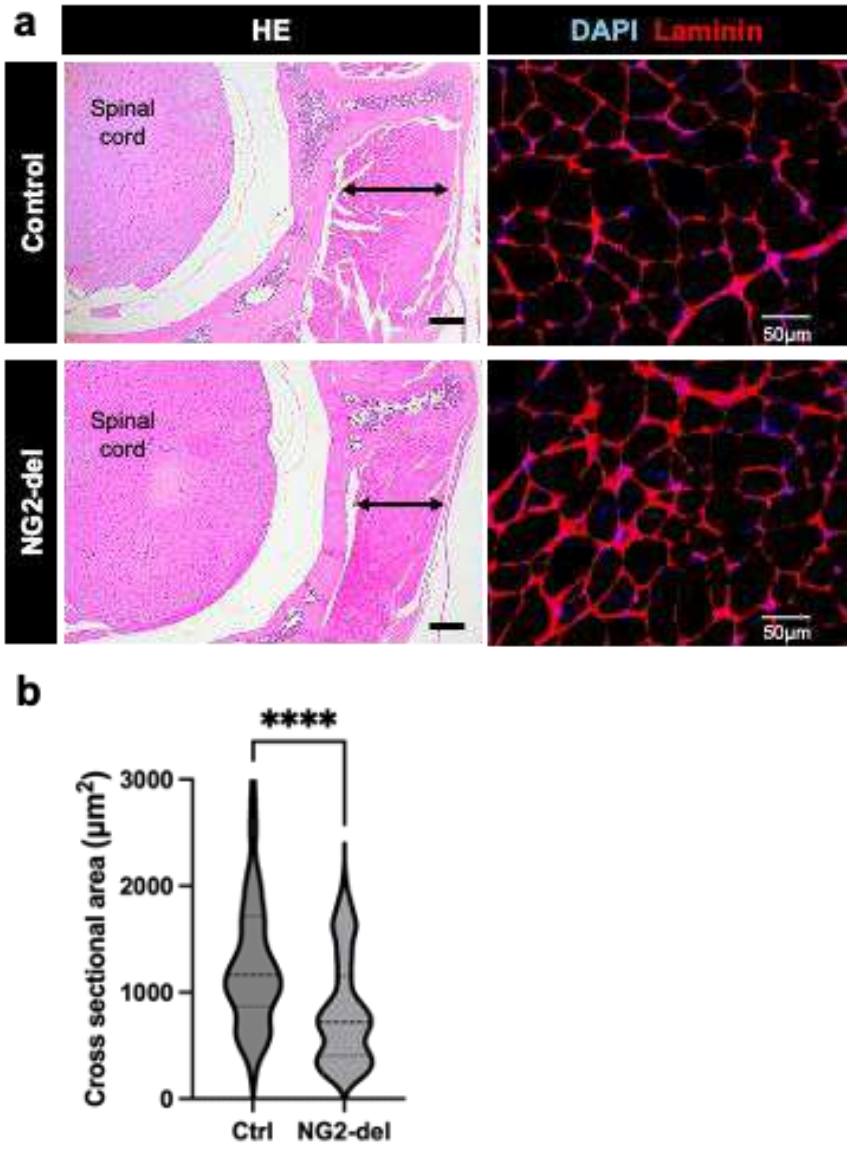


Fig. 3 NG2$^+$ cell depletion induced atrophy in the medial region of the erector spinae muscle

a. Representative H&E-stained images of the erector spinae muscle (ESM) (*arrow*) at the Thoracic vertebra 12 level, 2 months after NG2$^+$ cell depletion, showing marked atrophy of muscle bundles in NG2-del. Immunofluorescence images of the ESM. Laminin staining was used to delineate myofiber boundaries. Nuclei were counterstained with DAPI. Scale bar=200 μm**. b.** Quantification of myofiber cross section area (CSA) in the ESM at 2 months after NG2$^+$ cell depletion. CSA was significantly reduced in NG2-del compared with controls (Ctrl). The values are presented as the mean ± SEM (n=4), ****$P < 0.0001$

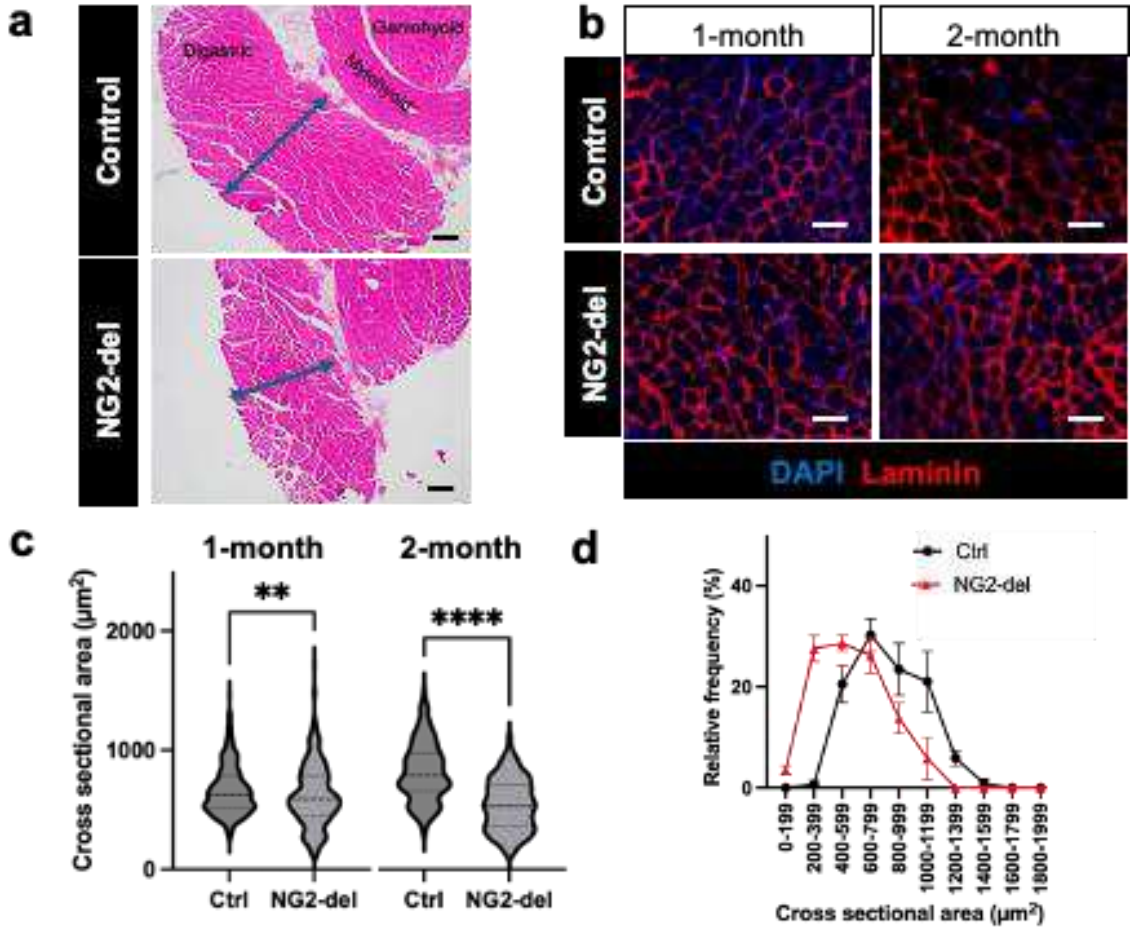


Fig. 4 NG2$^+$ cell depletion caused time-dependent progressive atrophy of the digastric muscle

a. Representative H&E-stained images of the digastric muscle (DIG) (*arrow*) at 2 months after NG2$^+$ cell depletion. Compared with controls, NG2$^+$ cell-depletion mice showed conspicuous thinning of the entire muscle bundles. Scale bar = 200 μm. **b.** Laminin immunofluorescence images of the DIG at 1 and 2 months after NG2$^+$ cell depletion. Nuclei were counterstained with DAPI. Scale bar = 50μm. **c.** Quantitative analyses of myofiber cross section area (CSA) at 1 and 2 months after NG2$^+$ cell depletion. The values are presented as the mean ± SEM (n=4), $^{**}P < 0.01$, $^{****}P < 0.0001$. **d.** CSA distribution in NG2-del and control mice (Ctrl) at 2 months after cell depletion.

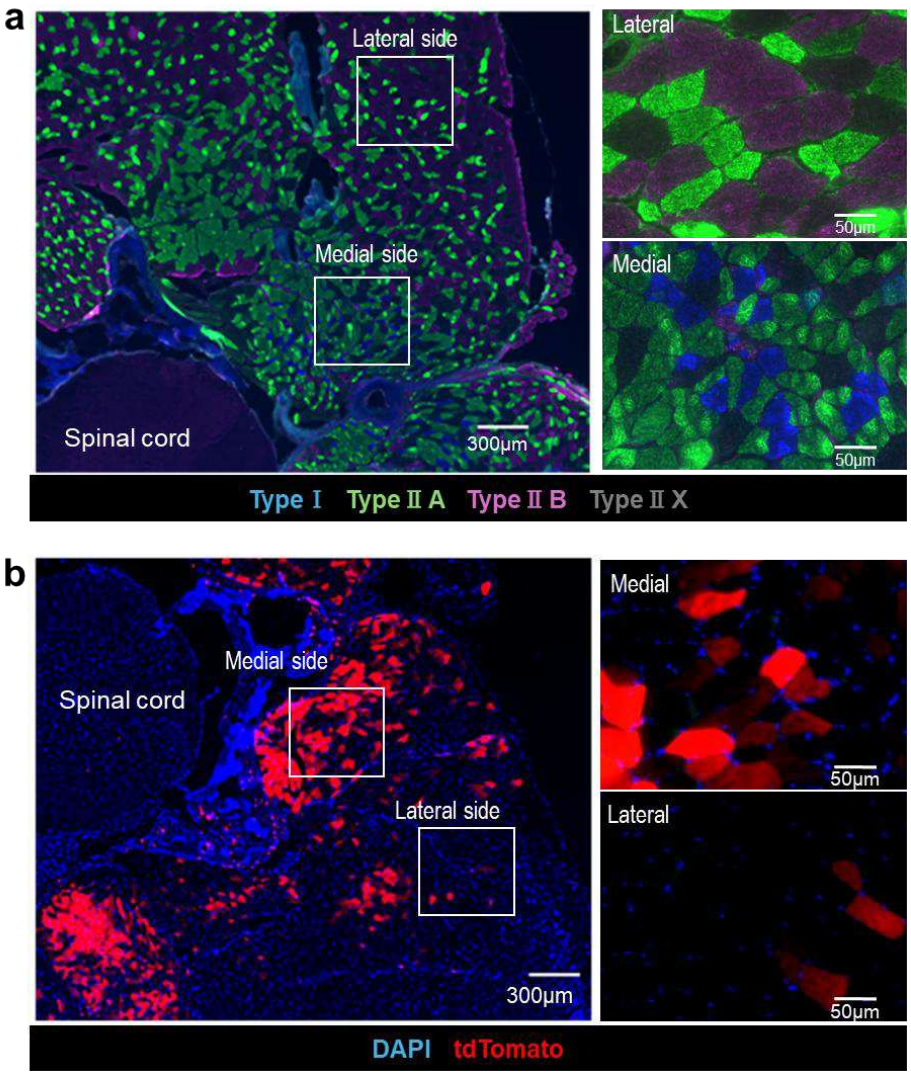


Fig. 5 Regional differences in myofiber-type composition and NG2$^+$ cell lineage–derived tdTomato$^+$ myofiber appearance within the erector spinae muscles

a. Low-magnification immunostaining images of the erector spinae muscles (ESM) indicating the medial and lateral regions analyzed, along with representative images for myofiber-type identification (right panel). The medial ESM was enriched in type I (slow-twitch) fibers, whereas the lateral ESM contained a higher proportion of type IIB (fast-twitch) fibers. **b.** For NG2$^+$ cell lineage tracing, NG2-CreERT;Rosa tdTomato mice treated with Tam. Representative images showed NG2$^+$ cell lineage–derived tdTomato$^+$ myofibers in the medial and lateral regions of the ESM. tdTomato$^+$ myofibers were more abundant in the medial ESM than in the lateral ESM, indicating region-specific differences in NG2$^+$ cell-lineage contribution.

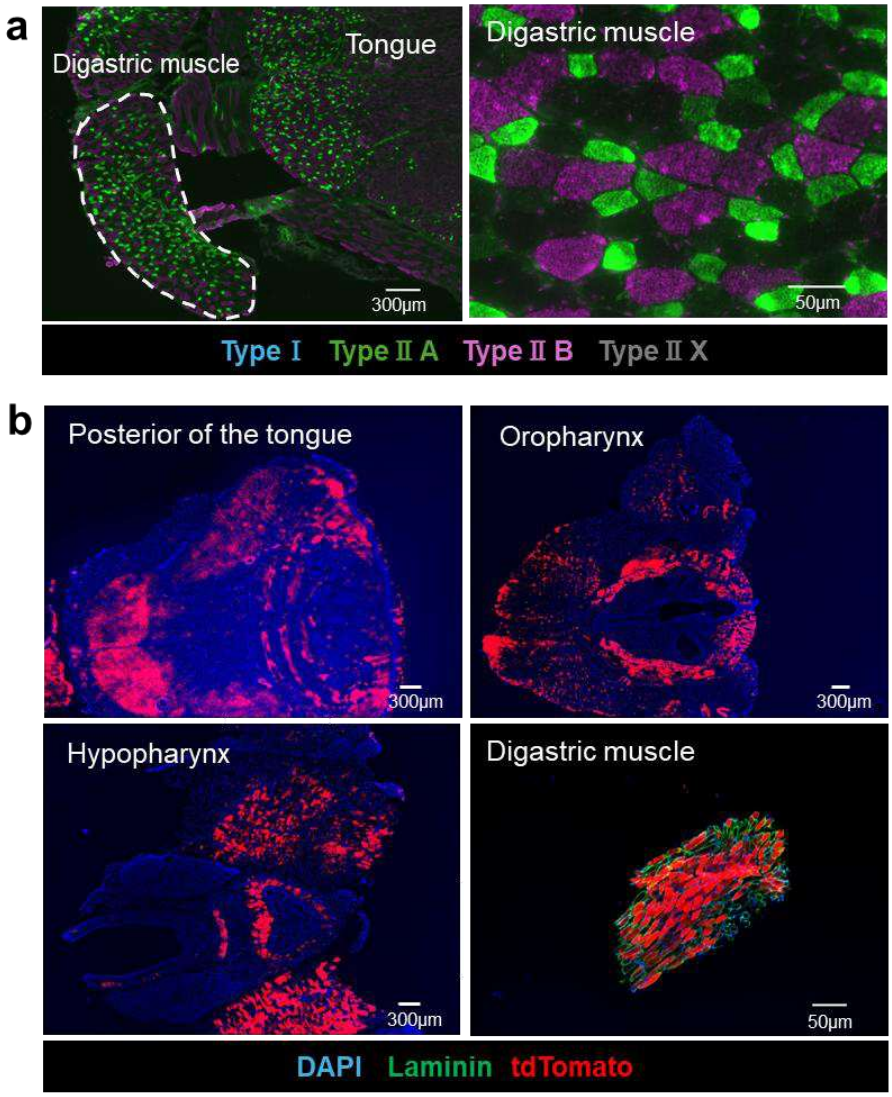


Fig. 6 Myofiber-type composition of the digastric muscle and widespread appearance of NG2$^+$ cell lineage-derived tdTomato$^+$ myofibers in pharyngeal regions

a. Low-magnification immunostaining images of the tongue and digastric muscle (DIG), with representative high-magnification images for myofiber-type identification in the DIG (right panel). DIG lacked type I fibers and consisted predominantly of type IIA, type IIX, and type IIB fibers, consistent with a fast-twitch dominant profile. **b.** NG2$^+$ cell lineage–derived tdTomato$^+$ myofibers were observed broadly across the pharyngeal region. High-magnification images of the DIG revealed that most myofibers were tdTomato$^+$, indicating extensive NG2$^+$ cell-lineage contribution to this muscle.

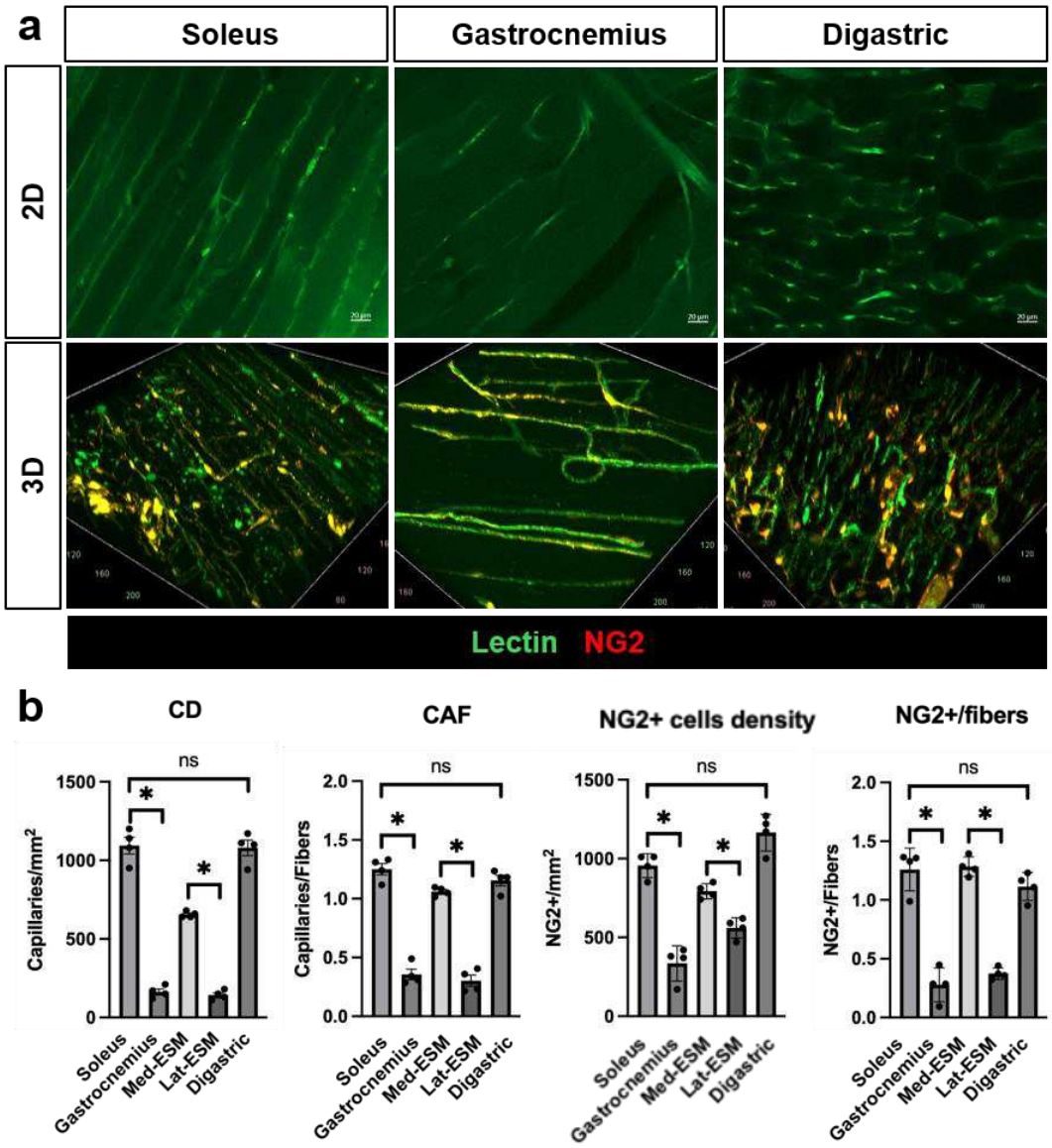


Fig. 7 Distribution of microvasculature and NG2$^+$ cell across skeletal muscle groups

a. Three-dimensional (3D) images illustrating the spatial relationship between capillaries and NG2$^+$ cells. Representative 2D lectin-labeled sections and corresponding confocal 3D-images of cleared muscle tissues (soleus, gastrocnemius, and digastric muscle) from lectin-injected NG2-DsRed mice are shown. **b.** Based on lectin labeling and NG2-DsRed signals, densities of capillaries and NG2$^+$ PCs were quantified as the number of capillaries or PCs per unit area and per myofiber, respectively. The values are presented as the mean ± SEM (n=4), *$P < 0.05$, ns = not significant

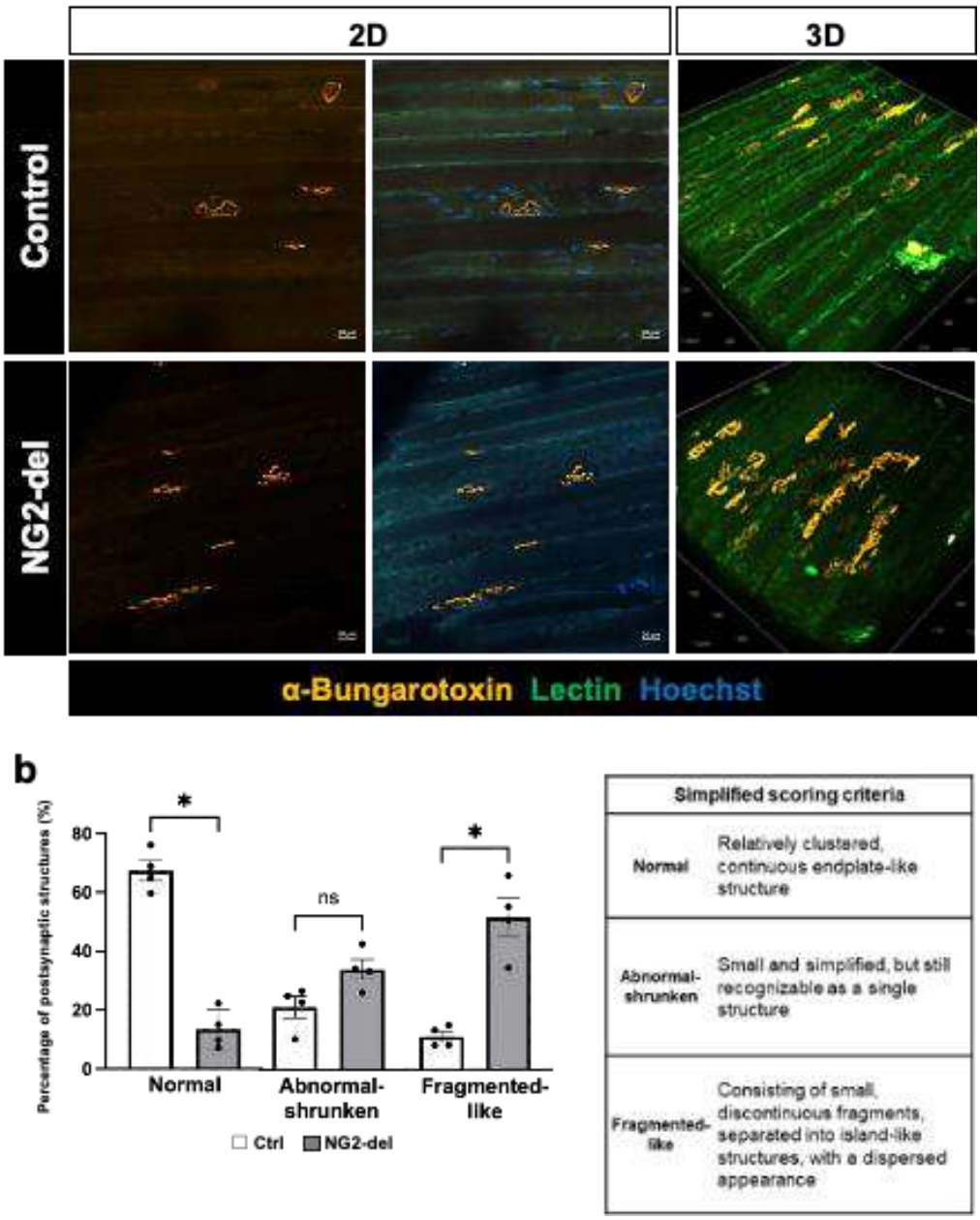


Fig. 8 NG2$^+$ cell depletion induced instability of neuromuscular junction (NMJ)

a. Representative images of the acetylcholine receptors (AChRs) labeled with a-bungarotoixn in the digastric muscles at 2 months after NG2$^+$ cell-depletion (NG2-del). Microvasculature and nuclei were stained by FITC-conjugated lection, and Hoechst respectively. **b.** The proportion of NMJ, identified as AchRs clusters, exhibiting defined morphological abnormalities was quantified. The values are presented as the mean ± SEM (n=4), *$P < 0.05$.

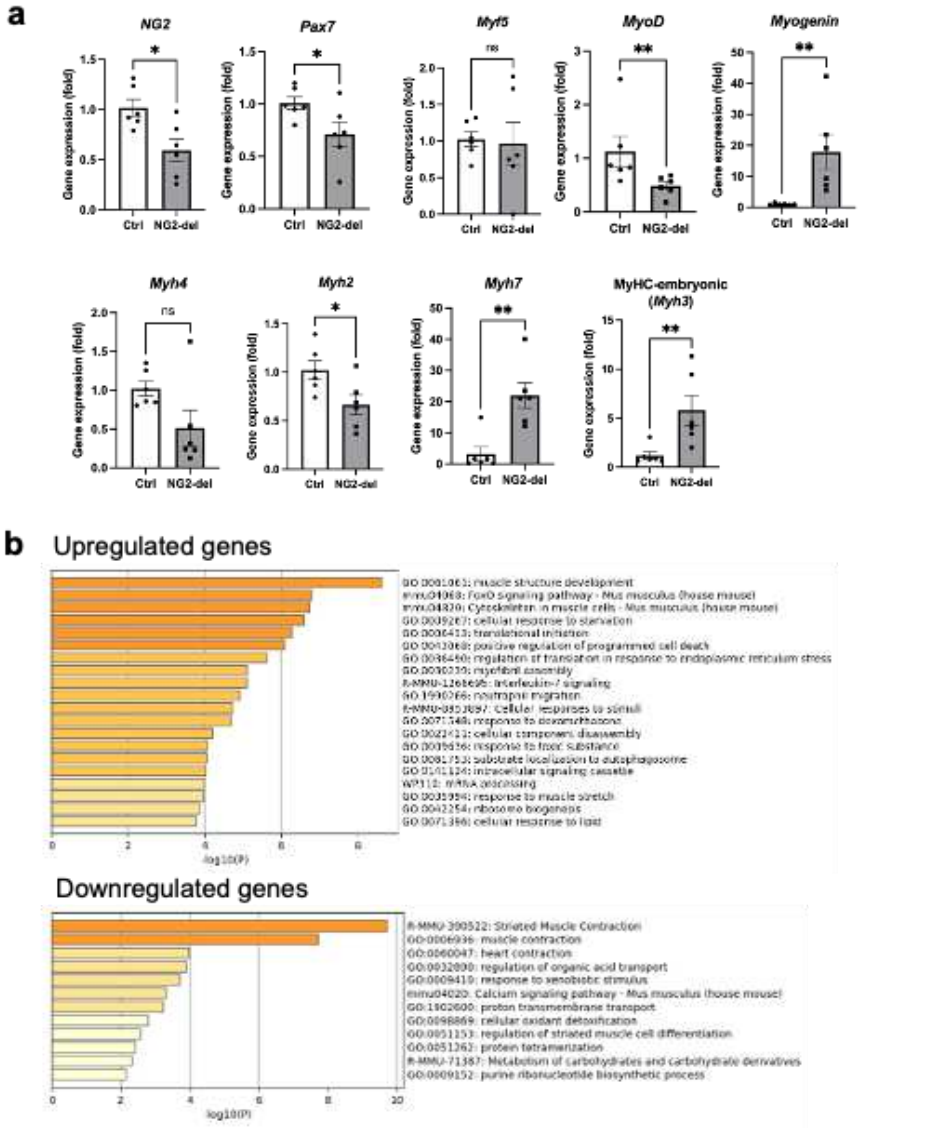


Fig. 9 Transcriptional changes in the digastric muscle following NG2$^+$ cell depletion

After 1 month of NG2$^+$ cell depletion, relative mRNA expression levels of indicated genes in the digastric muscle (DIG) were compared between control and NG2$^+$ cell-depletion (NG2-del) groups using quantitative PCR. Expression levels were normalized to the endogenous reference gene *18SrRNA*. Values were calculated as fold changes relative to the control group (Ctrl) and are presented as the mean ± SEM (n=6), **P* < 0.05, ***P* < 0.01, ns = not significant. **b.** Gene Ontology (GO) Biological Process enrichment analysis of differentially expressed genes. Microarray profiling was performed on the digastric muscle from NG2-del and Ctrl at 1 month after Tam-treatment. The top enriched GO Biological Process terms for upregulated and downregulated genes are shown; bar length indicates the number of genes (gene count) assigned to each term.

Table 1. Transcriptomic changes in the digastric muscle following NG2$^+$ cell depletion

Fold change (NG2-del/Ctrl): Up, * ≥ 2, ** ≥ 4, *** ≥ 8; Down, * ≤ 0.5, ** ≤ 0.25, *** ≤ 0.125.

Group	Symbol	Gene description	Normalized expression		Fold change (NG2-del/Ctrl)		
			Ctrl	NG2-del	Ratio	Up	Down
Cell markers	***NG2***	chondroitin sulfate proteoglycan 4	24	18	0.70		
	PDGFRβ	platelet derived growth factor receptor beta	103	93	0.90		
	PDGFRα	platelet derived growth factor receptor alpha	370	338	0.90		
	Pax3	paired box 3	5	4	0.70		
	Pax7	paired box 7	ND	ND	1.00		
	Acta1	actin alpha 1, skeletal muscle	42120	15983	0.40		*
	Acta2	actin alpha 2, smooth muscle	1737	1296	0.80		
Myogenesis	***Myf5***	myogenic factor 5	10	10	1.00		
	Myf6	myogenic factor 6	1128	1925	1.70		
	Myog	myogenin	24	356	14.80	***	
Sarcomeric-related genes	***Myh3***	myosin heavy chain 3, skeletal muscle, embryonic	11	72	6.40	**	
	Myh4	myosin heavy chain 4, skeletal muscle, adult	14843	8485	0.60		
	Myh2	myosin heavy chain 2, skeletal muscle, adult	17072	7709	0.50		*
	Myh7	myosin heavy chain 7, cardiac muscle, beta	258	413	1.60		
	Myl4	myosin light chain 4	55	928	16.90	***	
	Tnni2	troponin I type 2, skeletal, fast	42719	17370	0.40		*
	Tnnt2	troponin T2, cardiac	4	98	4.50	***	
Nerve/Neurogenesis	***Ncam1***	neural cell adhesion molecule 1	6	18	3.00	*	
	Ninj1	ninjurin 1	81	143	1.80		
	Cntnap1	contactin associated protein 1	4	7	1.90		
NMJ-related genes	***Musk***	muscle-associated receptor tyrosine kinase; central postsynaptic organizer for AChR clustering	20	17	0.80		
	Rapsn	receptor-associated protein of the synapse; AChR-anchoring scaffold protein	36	29	0.80		
	Agrn	agrin, canonical NMJ organizer	47	36	0.80		
	Lrp4	low density lipoprotein receptor-related protein 4	19	22	1.20		
	Dok7	downstream of tyrosine kinase 7	10	18	1.90		
Denervation-related genes	***Runx1***	RUNX family transcription factor 1	15	39	2.60	*	
	Fbxo32	F-box protein 32 (atrogin-1)	325	1138	3.50	*	
	Trim63	tripartite motif containing 63 (MuRF1)	25	68	2.70	*	
Hypoxia/Angiogenesis	***VEGF***	vascular endothelial growth factor A	117	85	0.73		
	Hif1a	hypoxia inducible factor 1 subunit alpha	64	91	1.41		
	Bnip3	BCL2 interacting protein 3	1031	1693	1.64		
	Pdk1	pyruvate dehydrogenase kinase 1	99	97	0.97		
	Slc2a1	solute carrier family 2, member 1	52	55	1.07		

Supplementary Files

This is a list of supplementary files associated with this preprint. Click to download.

- Satoetalmaterialinformation09162026.xlsx
- Satoetaldatasets9132026.xlsx